The Journal of Chemical Physics

Sub-nanosecond secondary geminate recombination in mercury halides HgX_2 (X = I, Br) investigated by time-resolved x-ray scattering

Cite as: J. Chem. Phys. **151**, 054310 (2019); https://doi.org/10.1063/1.5096422
Submitted: 18 March 2019 . Accepted: 24 June 2019 . Published Online: 05 August 2019

Denis Leshchev, Dmitry Khakhulin, Gemma Newby, Hosung Ki, Hyotcherl Ihee, and Michael Wulff

View Online Export Citation CrossMark

ARTICLES YOU MAY BE INTERESTED IN

Effects of polycrystalline birefringent grains on the morphology dependent resonance modes of a spherical resonator
Journal of Applied Physics **126**, 053102 (2019); https://doi.org/10.1063/1.5094333

Detecting coherent core-hole wave-packet dynamics in N_2 by time- and angle-resolved inner-shell photoelectron spectroscopy
The Journal of Chemical Physics **151**, 054107 (2019); https://doi.org/10.1063/1.5109867

Dynamical pruning of the non-equilibrium quantum dynamics of trapped ultracold bosons
The Journal of Chemical Physics **151**, 054108 (2019); https://doi.org/10.1063/1.5104344

Challenge us.
What are your needs for periodic signal detection?
Zurich Instruments
Watch

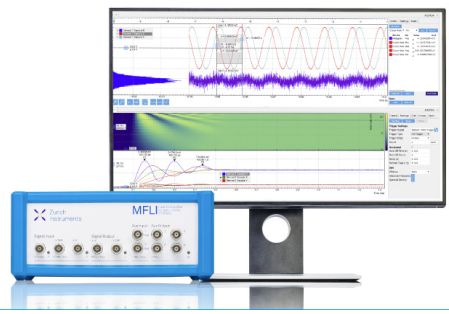

© 2019 Author(s).

The Journal of Chemical Physics ARTICLE scitation.org/journal/jcp

Sub-nanosecond secondary geminate recombination in mercury halides HgX_2 (X = I, Br) investigated by time-resolved x-ray scattering

Cite as: J. Chem. Phys. 151, 054310 (2019); doi: 10.1063/1.5096422
Submitted: 18 March 2019 • Accepted: 24 June 2019 •
Published Online: 5 August 2019

View Online Export Citation CrossMark

Denis Leshchev,[1,a] Dmitry Khakhulin,[2] Gemma Newby,[1] Hosung Ki,[3,4] Hyotcherl Ihee,[3,4] and Michael Wulff[1,b]

AFFILIATIONS

[1]European Synchrotron Radiation Facility (ESRF), 71 Avenue des Martyrs, 38000 Grenoble, France
[2]European XFEL GmbH, Holzkoppel 4, D-22869 Schenefeld, Germany
[3]Center for Nanomaterials and Chemical Reactions, Institute for Basic Science (IBS), Daejeon 305-701, South Korea
[4]Department of Chemistry and KI for the BioCentury, Korea Advanced Institute of Science and Technology (KAIST), Daejeon 305-701, South Korea

[a]**Current address:** Department of Chemistry, Northwestern University, Evanston, Illinois 60208, USA.
[b]**Author to whom correspondence should be addressed:** wulff@esrf.fr

ABSTRACT

In this work, we present a detailed investigation on the recombination dynamics of mercury halides HgX_2 (X = I, Br) in acetonitrile solution after UV-induced photodissociation. The study is performed by combining time-resolved wide-angle x-ray scattering (TRWAXS) and optical transient absorption spectroscopy. Up to 68% of the UV (266 nm) photodissociated HgX and X radicals that escape the solvent cage surrounding parent HgX_2 recombine within a nanosecond after photodissociation. In contrast to classical primary geminate recombination, occurring on much faster time scales, we interpret the sub-nanosecond recombination channel as secondary geminate recombination (SGR), also referred to as diffusion-limited geminate recombination. The family of triatomic mercury halides therefore represents an important class of molecules to study chemical mechanisms of solvent-dependent SGR by TRWAXS. The methodology described here allows for direct mapping of the time-dependent inter-radical distance distribution function, a critical parameter for the assessment of the SGR dynamics in solution phase and solvation in general.

Published under license by AIP Publishing. https://doi.org/10.1063/1.5096422

INTRODUCTION

The solvent plays a determining role in the yield, rate, and outcome of chemical reactions in solution. For photodissociation and recombination reactions, collisions between the solute fragments and the solvent molecules result in more complex radical recombination dynamics compared to their gas phase analogs. For the simplest systems, the recombination of radicals proceeds via three different channels.[1] First, upon photodissociation, a portion of the newly formed radicals bounces off the surrounding solvent cage and undergoes so-called primary geminate recombination (PGR) on the sub-picosecond time scale. Second, a fraction of the photodissociated radicals that initially escaped the solvent cage or the first solvation shell will diffuse and reside in its proximity until they eventually recombine geminately with their partner radicals to reform the parent molecule. This channel is called secondary geminate recombination (SGR), and it occurs within tens to hundreds of picoseconds after the dissociation event.[2–5] Finally, the radicals that did not undergo PGR or SGR may recombine nongeminately (NGR) on the time scales from nanoseconds to seconds or longer, depending on the physical properties of the solutes and the solvent, as well as the concentration of the radicals.

All three recombination channels have been investigated in detail for a number of molecular systems providing insights into the microscopic aspects of solution phase reactivity.[1,6–10] However, due to the limited number of SGR studies, the exact mechanism and

Published under license by AIP Publishing

physical interpretation are still unclear and being disputed. From a theoretical point of view, two approaches have been proposed.[2] The first description of SGR is based on the diffusion equation approach, where the liquid is assumed to be a structureless uniform medium. Shin and Kapral argued, however, that right after photodissociation, the radicals are typically separated by only a few solvent molecules, which invalidates the continuum model for describing the solvent-solute interactions. Therefore, in the second model they proposed a kinetic approach that takes into account the collisional character of the solvent-solute interactions. Both the diffusion and kinetic theories allow us to calculate the recombination probabilities of radicals as a function of time, which depend on their initial inter-radical separation, the macroscopic diffusion coefficients, and the in-cage recombination rate constants. Both theories predict nonexponential population kinetics; however, the kinetic approach results in slower recombination rates on short time scales as compared to the diffusion model due to strong solvent caging.[2] Theoretical simulations of SGR using Monte Carlo methods supported the diffusion model; however, the agreement was likely due to omission of the caging properties of the solvent.[11]

A few studies addressed the SGR channel experimentally, where it was attempted to compare predictions from the diffusion theory with spectroscopically measured radical concentration kinetics. In the study of the tetraphenylhydrazine photolysis, it was reported that theoretical parameters, such as the initial inter-radical separation and in-cage recombination rates, are highly correlated and cannot be determined based solely on the kinetic traces.[3] Further works on azo compounds and phenylthiyl radicals attempted to circumvent this problem by assuming a solvent-independent inter-radical separation distance, as well as by measuring the SGR rates and yields as a function of solvent viscosity to impose an additional constraint on the diffusion coefficients.[4,5] While qualitative agreement between the diffusion model and the experiments was found, no direct comparison between the diffusion and the kinetic models was performed. More recently, the diffusion-based model of SGR was proposed and applied for describing the recombination of a protein with aromatic disulfide radicals.[12,13] It was concluded that the recombination is driven by the protein motions along a rough potential energy surface rather than by a random diffusion in solution.[12,13] Spectroscopic studies on a series of inorganic compounds,[14] as well as alkylcobalamins,[15] addressed the effect of radical mass, size, and solvent on the ratio between SGR and PGR yields. Although these works addressed some specific aspects of the SGR dynamics, the understanding of the underlying mechanisms is still limited. Developing a general quantitative model of SGR will help to elucidate the role of the solvent environment in the radical reactivity and determine the time- and the length-scale limits for validity of the continuum model.

In this work we focus on the identification of a class of systems and tools that allow getting a deeper understanding of SGR, such as distinguishing between kinetic and diffusion processes. Here we investigate the recombination dynamics of the radicals formed after UV photodissociation of mercury halides HgX_2 (X = I, Br) in acetonitrile by optical transient absorption (OTA) spectroscopy and time-resolved wide-angle x-ray scattering (TRWAXS), also known as time-resolved x-ray liquidography (TRXL).[7,16] The UV excitation of HgX_2 in solution results in two-body dissociation for HgI_2 and in a mixture of two- and three-body dissociation for $HgBr_2$.[17–19] Since the vibrational and rotational relaxations of the photoproducts are completed within the first few picoseconds after the excitation,[20–23] these processes have no effect on the SGR process occurring on time scales between 10 ps and 1 ns.[1] The combination of picosecond OTA spectroscopy and synchrotron TRWAXS provides a complete set of observables to study the picosecond electronic kinetics and the transient structural dynamics of radicals during SGR. We further discuss a strategy for a deeper investigation of SGR by tracking the time-dependent inter-radical distance by femtosecond TRWAXS at free electron lasers.

METHODS

Sample preparation

HgI_2 and $HgBr_2$ powders (≥99.0% purity) and acetonitrile (≥99.5% purity) were purchased from Sigma-Aldrich and used without further purification. The samples were prepared by dissolving the powders in acetonitrile to optimal concentrations for OTA and TRWAXS measurements (see below).

OTA experiments

The OTA data were acquired using an optical pump/optical probe setup based on a Ti:sapphire femtosecond Legend-II amplifier laser from Coherent. The 267 nm pump beam and 493 Hz pulse repetition rate was focused on the sample to a round spot of about 0.7 mm in diameter (FWHM). The probe beam at 400 nm and with 986 Hz pulse repetition rate was focused to a 0.3 mm round spot (FWHM). The pulse energies of the pump and the probe were 10 μJ/pulse and 0.2 μJ/pulse, respectively. The pulse duration for both pump and probe was 1.2 ps. The sample was flown through a sapphire nozzle forming a flat liquid sheet with 300 μm thickness. Changes in the transmitted probe pulse were measured as a function of the pump-probe delay by moving a mechanical delay stage and detecting the probe intensity with a Si photodiode. The transient signal from the photodiode was gated and digitized by a combination of a boxcar integrator and a lock-in amplifier (Stanford Research Systems). Acetonitrile solutions of 0.5 mM and 2 mM concentrations were used for the HgI_2 and the $HgBr_2$, respectively. Measurements were done at room temperature.

TRWAXS experiments

The TRWAXS data for the HgI_2 and the $HgBr_2$ solutions in acetonitrile were collected at the ID09 beamline of the European Synchrotron Radiation Facility using the standard TRWAXS experimental protocol described elsewhere.[7] The experiments were performed using the same laser system as the one used for OTA. The photodissociation was triggered by 267 nm excitation and probed by 100 ps x-ray pulses collecting scattering patterns on a 2D camera placed downstream the sample. For HgI_2, the laser pulses with energy 150 μJ were focused onto a round spot with a FWHM of 210 μm, giving a fluence of 0.32 J/cm^2. For $HgBr_2$, the laser pulses with energy 80 μJ were focused onto a round spot with a FWHM of 150 μm, giving a fluence of 0.33 J/cm^2. In both cases, an x-ray beam with a "pink" spectrum produced by the U17 undulator with a peak energy of 18 keV and a bandwidth of ~3% was focused to a 100 μm (H) × 60 μm (V) spot. The sample was flown through a sapphire nozzle to form a 300 μm thick flat liquid sheet with a flow

Published under license by AIP Publishing

speed of ~3 m/s so that each pump/probe event occurs in a fresh sample volume, given that the repetition rate of the stroboscopic pump-probe experiment was 986 Hz. The solution concentrations were 7 mM and 25 mM for the HgI_2 and $HgBr_2$ samples, respectively, resulting in an optical density of ~1 for each sample. The 2D scattering patterns were measured with a FreLoN 4M camera[24] 40.7 mm and 42.5 mm from the sample for HgI_2 and $HgBr_2$, respectively. Measurements were run at room temperature. The scattering images were azimuthally integrated, normalized, and reduced to difference scattering patterns using standard procedures.[7,25] The data were collected using the so-called "slicing" technique, i.e., the time-delay between the laser and x-ray pulses is scanned in steps of 10 ps which has the advantage of probing sub-100 ps dynamics as previously demonstrated.[26] For each scattering pattern, the average time delay between laser and x-ray pulses was recorded using a fast diamond (for x-rays) or GaAs (for laser) photodiode with ~100 ps and ~70 ps rise-times, respectively. The recorded images were sorted according to the measured time delays, which allowed for correction of long-term drifts in the beamline. The effect of the impulsive solvent heating was corrected using reference solvent responses collected using azo-dye solutions following the standard protocol.[27] The theoretical difference curves were calculated by the Debye equation using the molecular structures of HgX_2 and possible reaction products from the literature (see notes S1 and S2 in the supplementary material);[18,19] a table with structural parameters used for scattering signal calculations can be found in the supplementary material. The cage contribution was omitted since it has a little effect on the fitting results (see note S3 in the supplementary material), which is in agreement with previous experiments on similar solutions with high-Z solute atoms in organic solvents and when the analysis-relevant q-range extends well beyond 1 $Å^{-1}$.[7,18,28,29] The high quality of the fits shows that the chosen procedure is adequate for the current study. The fitting was performed according to the standard procedures;[7,19,25] the uncertainties listed for best fit values correspond to a 95% confidence interval.

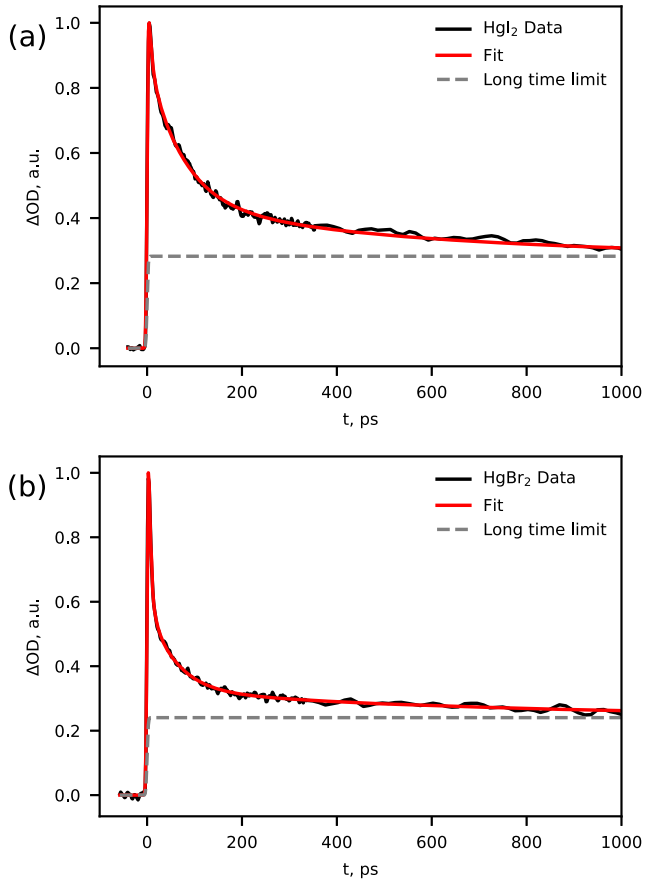

FIG. 1. (a) OTA time profiles obtained for HgI_2 in acetonitrile using 267 nm pump and 400 nm probe. (b) The same as (a) but for $HgBr_2$ in acetonitrile. The signals are normalized by the maximum observed values.

RESULTS

OTA spectroscopy

The OTA results for HgI_2 and $HgBr_2$ in acetonitrile using 267 nm pump and 400 nm probe are shown in Figs. 1(a) and 1(b). The 400 nm wavelength probes the band from the $X \rightarrow B$ transition in the HgX radical (380–520 nm), which has been used before for characterizing relaxation processes in mercury halides.[22,30] The photolysis of both samples results in the appearance of a sharp increase in the absorption signal at time-zero, which first decays on the sub-10 ps time scale, then slowly decreases up to 250 ps, and decays even further up to 2 ns. To quantify the time scales of the decays, the signals were fitted with a triple exponential decay function: $A(t) = A_0 + A_1 \exp(-t/\tau_1) + A_2 \exp(-t/\tau_2) + A_3 \exp(-t/\tau_3)$. In the fitting procedure, the theoretical signal was convoluted with the instrument response function and corrected for time-zero. For HgI_2, we obtained the following decay constants: $\tau_1 = 7 \pm 2$ ps, $\tau_2 = 73 \pm 6$ ps, and $\tau_3 = 530 \pm 60$ ps, while for $HgBr_2$, the following decay constants were observed: $\tau_1 = 5 \pm 2$ ps, $\tau_2 = 56 \pm 4$ ps, and $\tau_3 = 730 \pm 100$ ps. The sub-10 ps lifetimes are attributed to ultrafast vibrational and rotational relaxations of the HgX radicals and the in-cage relaxation of the photoproducts, which include radicals undergoing PGR and internal conversion (IC) of excited HgX_2 molecules directly to the ground state. The longer lifetimes indicate a presence of slower relaxation dynamics in the systems that were not reported in the previous spectroscopic studies. These long-lived photoproducts were identified in the TRWAXS measurements.

TRWAXS

The TRWAXS signals for the HgI_2 dissociation at early time delays between −100 ps and 1 ns, as well as the q-integrated absolute signal, are shown in Figs. 2(a) and 2(b). The rise of the signal around time zero is broadened by the instrument response function from the 100 ps x-ray pulse. The $q\Delta S(q, t)$ signal between 50 and 200 ps decays on the 100 ps time scale, which is followed by a further decrease on the nanosecond time scale. For $HgBr_2$, the rise of a strong signal around time-zero is followed by a sub-nanosecond decay and then plateauing on the nanosecond time scale [Figs. 2(c) and 2(d)]. In both cases, the fast decays indicate the presence of a rapid relaxation process, similarly to the OTA results; however, the assignment of the relaxation origin requires detailed

Published under license by AIP Publishing

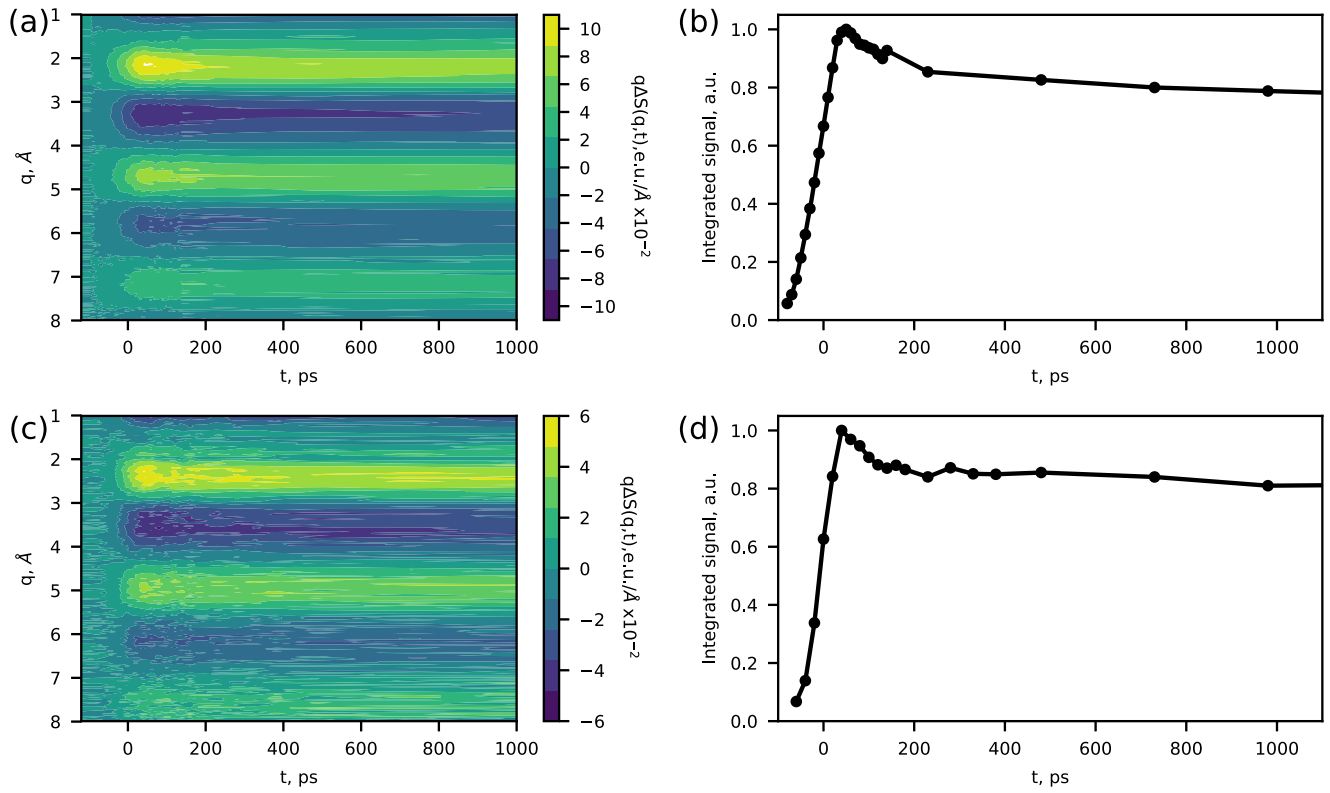

FIG. 2. (a) TRWAXS for HgI_2 in acetonitrile using 267 nm excitation. (b) Total absolute integrated TRWAXS signal for HgI_2 as a function of time. [(c) and (d)] The panels (c) and (d) are the same as (a) and (b), but for $HgBr_2$ in acetonitrile.

analysis of the scattering spectra based on the structural and kinetic models.

Previous analysis of the reaction energetics suggests that the following four channels are energetically allowed upon UV excitation of HgX_2 (X = Br, I):[18,19] (1) two-body dissociation resulting in the formation of HgX and X radicals, (2) three-body dissociation resulting in the formation of Hg and X radicals, (3) direct formation of molecular X_2 and a Hg radical, and (4) formation of the isomer HgX–X. While TRWAXS experiments on HgX_2 in methanol[18,19] have ruled out (3) and (4) in acetonitrile, the photochemistry of HgX_2 may differ. To evaluate the structural signatures of potential halide radicals upon dissociation, a linear combination fitting of the reduced difference scattering traces at early delays (70 ps and 60 ps) was performed using the published structures of the ground-state HgX_2 and its possible photoproducts (see note S1 in the supplementary material). For HgI_2, the best fit corresponds to simple two-body dissociation to HgI and I, while for $HgBr_2$, the analysis converges to a mixture of two- and three-body dissociation channels with a ratio of 4:1 and adding other photoproducts from the list of potential species does not improve the fit. The same type of analysis performed on the data from other time delays gives the same assignment of the photoproducts. However, for the later delays (>100 ns), the formation of small amounts of I_2 and Br_2 are observed due to the NGR of I and Br. These findings in acetonitrile are in agreement with earlier reports for methanol solutions.[18,19]

We also find that the refinement of the HgX_2 and HgX geometries yields structures in good agreement with previous calculations; however, some bending of the HgI_2 structure is observed. We tentatively attribute this to the effect of bending vibrations that result in effective shrinkage of the average I-I distance, which have been previously reported from electron diffraction and Coulomb explosion imaging measurements.[31–34]

The full concentration kinetics of the radicals were extracted by fitting the data at individual time points as shown in Fig. 3. For HgI_2, we observe a rapid decay of the initial HgI and I concentrations by 200 ps and an additional weaker decay between 200 ps and 3 ns. For $HgBr_2$, a similar rapid decay of the HgBr and Br concentrations on the 100 ps time scale is observed as in HgI_2 although the Hg radical does not show a significant reduction within the first 100 ps. For both HgI_2 and $HgBr_2$, the concentration kinetics on the nanosecond to microsecond time scales indicate further recombination which can be attributed to NGR as reported previously.[18,19] Since the rapid recombination occurs from a few tens of picoseconds to a nanosecond, the concentration decay of the HgX and X radicals cannot be attributed to the PGR that is usually complete within picoseconds inside the first solvation shell.[1] On the other hand, the 100 ps time scale from the rapid recombination of the HgX and X radicals is of the same order as reported for the SGR process for other small molecules.[3–5] We therefore assign it to SGR, i.e., to diffusion-limited geminate recombination.

Published under license by AIP Publishing

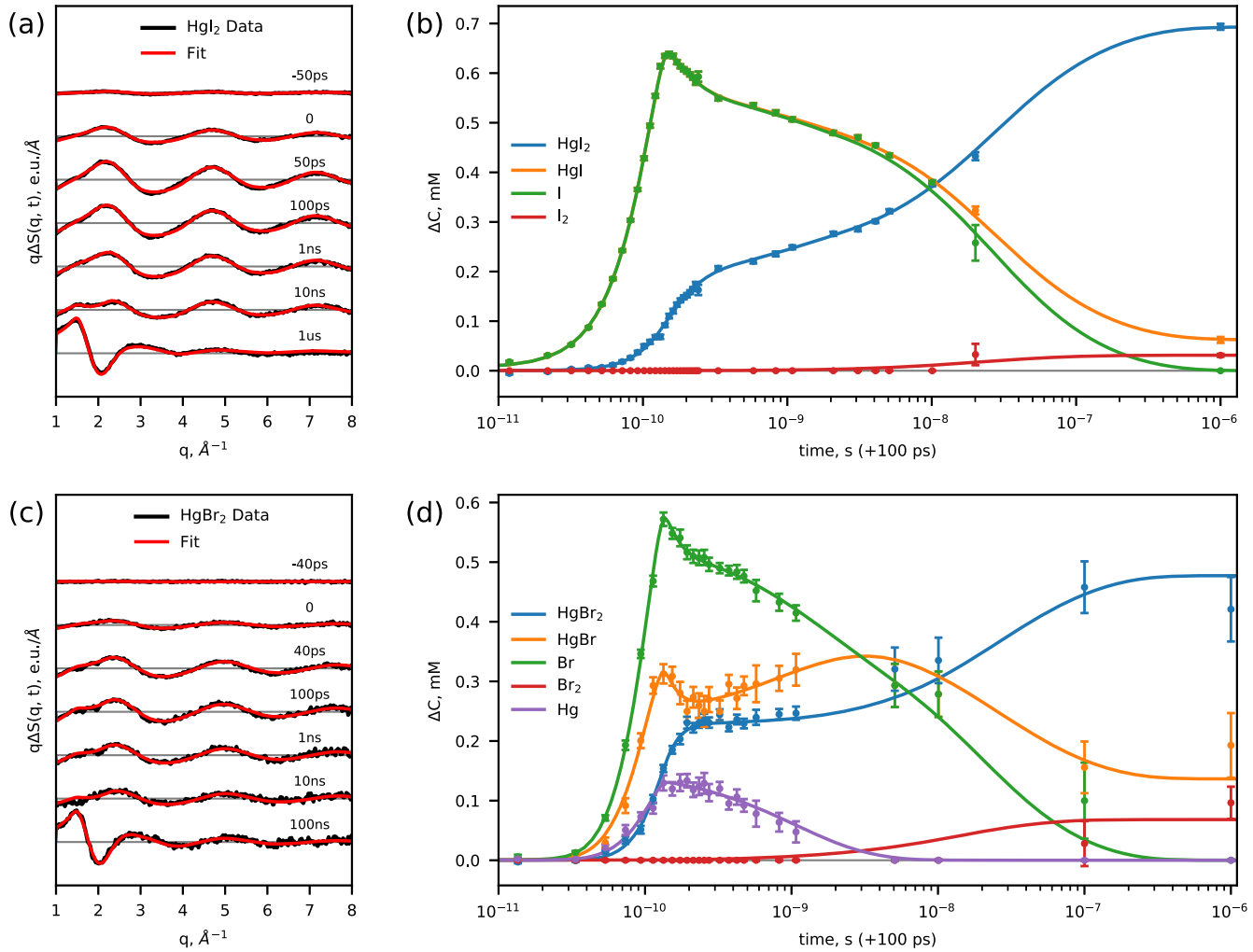

FIG. 3. (a) Fitting of select TRWAXS curves for HgI_2 in acetonitrile. (b) Transient concentrations of the HgI, I, and I_2 radicals as a function of time from TRWAXS (circles) and kinetic fits (solid line). Note that the time axis is shifted by +100 ps to include negative time delays on a logarithmic scale. (c) Fitting of select TRWAXS curves for $HgBr_2$ in acetonitrile. (d) Transient concentrations of HgBr, Br, Br_2, and Hg as a function of time from TRWAXS (circles) and kinetic fits (solid line). The time axis is shifted by +100 ps to include negative time delays on a logarithmic scale.

To quantitatively assess the SGR time scales and the fraction of radicals participating in this process, we performed a kinetic fitting of the transient concentrations. The simplest diffusion-based description of SGR predicts a nonexponential decay of the concentrations: free radicals typically undergo rapid recombination on short time scales with the rate proportional to $t^{-1/2}$ followed by a slower phase which decays at a rate proportional to $t^{-3/2}$.[2,12,13] Since, as discussed above, the fitting of SGR models is not feasible due to the high correlation between the parameters, a phenomenological double exponential model with a "fast" and "slow" phase can be used. This description is in line with the simple model employed for the description of the OTA results presented above. We note, however, that the OTA data required a triple exponential model, where one of the decays is associated with ultrafast relaxation on the picosecond time scale. The fastest component is not needed for the description of the TRWAXS data since the slicing technique utilized in this work (see Methods) can only resolve processes as short as a few tens of picoseconds. Moreover, it appears that for $HgBr_2$, the "slow" phase of the SGR decay is not determined from the data due to the limited signal-to-noise ratio. To fit the NGR process at longer time delays as well as the Hg concentration on the nanosecond time scale, we use a standard set of differential equations describing second order reactions (see note S4 in the supplementary material for details). The fits to the transient radical concentrations are shown in Figs. 3(b) and 3(d) for the HgI_2 and $HgBr_2$, respectively. Additionally, as in previous works,[18,19] from the difference between the expected and observed temperature rise at 1 μs, we indirectly infer the in-cage relaxation yield for both molecules (see note S5 in the supplementary material for details), which includes radicals undergoing PGR and the decay of excited HgX_2 via IC. The best fit

Published under license by AIP Publishing

TABLE I. Photodissociation and recombination of HgX_2 in acetonitrile: Rates, yields, and lifetimes.

	HgI_2	$HgBr_2$
Excitation efficiency, primary geminate recombination, and dissociation channel yields		
Excited state fraction	0.20 ± 0.02	0.06 ± 0.01
In-cage recombination yield[a]	0.46 ± 0.06[b]	0.5 ± 0.2
Two-body dissociation yield[c]	1	0.78 ± 0.06
Three-body dissociation yield	0	0.22 ± 0.06
Secondary geminate recombination		
SGR yield[d]	0.33 ± 0.04 (TRWAXS) 0.68 ± 0.02 (OTA)	0.5 ± 0.2 (TRWAXS) 0.60 ± 0.02 (OTA)
Relative amplitude of the fast phase[e]	0.75 ± 0.10 (TRWAXS) 0.73 ± 0.06 (OTA)	1.0 (TRWAXS) 0.77 ± 0.08 (OTA)
Time constant of the fast phase, ps	70 ± 30 (TRWAXS) 73 ± 6 (OTA)	35 ± 20 (TRWAXS) 56 ± 4 (OTA)
Relative amplitude of the slow phase[e]	0.25 ± 0.10 (TRWAXS) 0.27 ± 0.06 (OTA)	0.0 (TRWAXS) 0.23 ± 0.08 (OTA)
Time constant of the slow phase (ps)	600 ± 300 (TRWAXS) 530 ± 60 (OTA)	... 730 ± 100 (OTA)
Nongeminate recombination		
$K^{NGR}_{HgX+X\rightarrow HgX_2}\left(M^{-1}\,s^{-1}\right)$	$(6.5 \pm 0.4) \times 10^{10}$	$(7.5 \pm 0.5) \times 10^{10}$
$K^{NGR}_{Hg+X\rightarrow HgX}\left(M^{-1}\,s^{-1}\right)$	...	$(2 \pm 1) \times 10^{12}$
$K^{NGR}_{X+X\rightarrow X_2}\left(M^{-1}\,s^{-1}\right)$	$(6 \pm 2) \times 10^{9}$	$(2 \pm 1) \times 10^{10}$

[a]The in-cage recombination yield is calculated as the ratio between concentrations of the molecules that undergo this channel and the excited molecules: $\frac{[HgX_2]_{PGR}}{[HgX_2]_{excited}}$.

[b]Combination of the OTA SGR yield with TRWAXS for HgI_2 results in in-cage recombination yield of 0.26 ± 0.06.

[c]The two-body dissociation yield is calculated as a ratio between the concentrations of HgX radicals and a sum of concentrations of HgX and Hg radicals, which escaped the initial cage: $\frac{[HgX]_{esc}}{[HgX]_{esc}+[Hg]_{esc}}$.

[d]The SGR yield is calculated as a ratio between the concentrations of HgX radicals that undergo SGR and those that undergo both SGR and NGR: $\frac{[HgX]_{SGR}}{[HgX]_{SGR}+[HgX]_{NGR}}$.

[e]The relative amplitudes of the fast and slow phases are calculated as ratios between the concentrations of the HgX radicals that undergo fast and slow phases, respectively, and the total concentration of the HgX radicals that undergo SGR: $f_{SGR,fast} = \frac{[HgX]_{SGR,fast}}{[HgX]_{SGR}}$ and $f_{SGR,slow} = \frac{[HgX]_{SGR,slow}}{[HgX]_{SGR}}$.

values of the reaction yields, time scales, and bimolecular diffusion coefficients for different recombination channels are summarized in Table I along with the analysis results of the OTA data.

While the TRWAXS data allow us to identify the origin of the rapid radical concentration as the SGR, the 100 ps width of the x-ray pulse in the current measurements causes a temporal smearing of the kinetics. This could bias the SRG amplitudes and time scales despite the analysis taking the instrument response function into account. To assess the potential errors arising from this smearing, we compared the SGR parameters from TRWAXS and OTA. For HgI_2, the relative amplitudes and time scales of the fast and slow phases obtained from OTA and TRWAXS agree within the uncertainty. Even for $HgBr_2$, where the TRWAXS could only resolve the fast component, the decay constant matches the OTA result. Notably, the overall SGR yield for $HgBr_2$ from the two measurements is in fair agreement, whereas for HgI_2, the TRWAXS estimate is almost twice lower compared to the OTA result. The exact origin of the latter disagreement may be addressed in future TRWAXS measurements performed with better temporal resolution, whereas in the present work, we will deem the OTA results as more reliable (see note S6 in the supplementary material for further details).

DISCUSSION

Our results demonstrate that the recombination of the radicals formed after photodissociation of HgX_2 is a complex process spanning multiple time scales and involving different mechanisms. Based on TRWAXS and OTA, we propose the following picture of the recombination dynamics in mercury halides. The overall reaction pathways for both molecules are schematically summarized in Fig. 4. Upon photodissociation of HgI_2, a quarter of the excited HgI_2 molecules relaxes back to the ground state in-cage. This includes the photofragments that undergo PGR as well as the excited HgI_2

Published under license by AIP Publishing

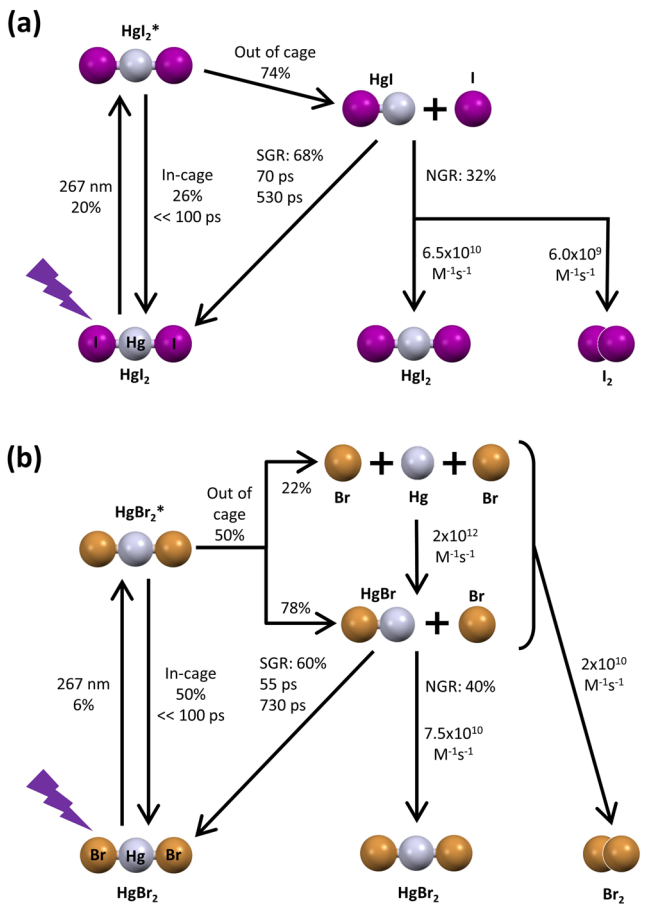

FIG. 4. Global reaction scheme derived from TRWAXS and OTA measurements for (a) HgI_2 and (b) $HgBr_2$ in acetonitrile. The in-cage and out of cage percentages represent the fractions of the excited HgX_2 molecules undergoing either in-cage relaxation or dissociation into radicals that escape the cage. For $HgBr_2$, percentages of radicals that escape the cage and undergo two- and three-body dissociation are shown. The SGR and NGR percentages represent fractions of initially formed HgX radicals that undergo SGR and NGR.

molecules that decay back to the ground state via IC and then vibrationally cool down. About 68% of the HgI fragments that have left the cage initially diffuse in proximity until they recombine with I via the SGR within the first nanosecond. Most of the rest HgI and I radicals undergo NGR to form HgI2, whereas 8% of all I radicals that initially escaped the cage form molecular I_2. For $HgBr_2$, about 50% of the excited molecules recombine in-cage, and the rest dissociates into the fragments that escape the cage, of which about 78% undergo the two-body dissociation and the 22% undergo the three-body dissociation. 60% of the HgBr radicals formed in the two-body dissociation recombine with Br through SGR. Hg and Br form HgBr which then recombines with the remaining Br radicals to form $HgBr_2$ via NGR. 17% of Br radicals that initially escaped the cage form molecular Br_2.

In contrast to the present work, previous TRWAXS investigations of HgX_2 photodissociation reactions did not report the SGR process.[18,19] This might be due to one of the two following reasons. First, the previous works used methanol as solvent, which has a higher dynamic viscosity compared to acetonitrile (η_{MeCN} = 0.34 cP and η_{MeOH} = 0.54 cP) and therefore might result in a smaller SGR yield. It has been shown for other molecules that the viscosity has a drastic effect on the probability for a radical to escape the solvent cage and also affects the relative yields of SGR and NGR.[3–5] Second, previous experiments were mainly focused on NGR and had limited sampling of the early time delays, which could obstruct the observation of the rapid radical recombination from SGR. Additionally, the observation of the SGR process requires the time "slicing" technique,[26] where the time delays around time zero are finely scanned in steps of 10 ps as in the present work.

A comparison of the SGR and NGR rates in HgI_2 and $HgBr_2$ allows us to assess the main difference in the recombination of the two systems. For NGR, one would expect that the radical size is the main factor affecting the bimolecular diffusion rates. This indeed holds true for some of the radicals; for example, the HgI/I recombination rate is slower than that of the HgBr/Br pair, where the Br atom is smaller than the I atom. On the other hand, we find that I/I and Br/Br pairs recombine slower than HgI/I and HgBr/Br, where the latter radicals are larger compared to the former ones. We speculate that this effect is due to the strong interactions between the halogen atoms and the polar acetonitrile molecules, which are known to result in the formation of contact charge transfer complexes X:solvent (X = I, Br).[23,35,36] These interactions may lead to an effective increase in the X radical size and, hence, a decrease in the diffusion coefficient of the X radicals as compared to that of HgX. Similarly to the previous work in methanol,[19] we find that the recombination rate of the I/I pairs is slower than for Br/Br in acetonitrile, which may be interpreted as a size effect; however, strong interactions with the solvent have to be taken into account in order to understand the dependence of the recombination rates on the type of radical. Finally, we observe that the Hg radical has the highest recombination rate, indicating that Hg is the most mobile radical under our experimental conditions, which is likely due to its small size.

For SGR, the differences between HgI_2 and $HgBr_2$ cannot be explained in a simple way. The results indicate that the fast SGR phase, which constitutes the bulk of the recombination (see Table I), has a shorter time scale for HgBr/Br (55 ps) than for HgI/I (73 ps). While the higher diffusion rate of the first pair is a natural explanation for this effect, the same argument cannot be applied to the slow component. For the slow SGR phase, the HgBr/Br recombination time scale (730 ps) is larger than that for HgI/I (530 ps), showing an inverse trend compared to the fast SGR phase. These observations suggest that SGR cannot be explained only in terms of diffusion rates. As mentioned earlier, the simplest SGR description indicates a highly nonexponential behavior, which is predicted based on the diffusion rate, in-cage radical recombination rates, and initial inter-radical separation distances. The difference between the dissociation mechanisms of HgI_2 and $HgBr_2$, i.e., two-body only and two- and three-body dissociation mixture, suggests a substantial difference between the dissociative potential energy surfaces. This difference might affect the distribution of kinetic energies between the HgX and X radicals, which in turn results in different initial radical separation distances and therefore different SGR rates. Finally, the TRWAXS results show no significant SGR for Hg/Br pair of radicals.

Published under license by AIP Publishing

Since the three-body dissociation is more energetically expensive and provides smaller kinetic energies for the photofragments, the initial separation distance for Hg/Br pairs is smaller compared to HgBr/Br pairs. The former, coupled to the high mobility of the Hg radical, substantially shortens the characteristic time scales of SGR for the Hg/Br pairs, likely making the Hg/Br SGR inaccessible in the present TRWAXS study.

The independent characterization of the inter-radical separation distance is a cornerstone for the understanding of the SGR process and would allow us to interpret the differences between SGR of HgI/I, HgBr/Br, and Hg/Br radical pairs in detail. The reported TRWAXS measurements cannot directly provide this important parameter due to the limited temporal resolution of the synchrotron setup. Indeed, the initially well-defined inter-radical distance distribution emerging upon photodissociation is only a few solvent molecule radii in width and it quickly broadens and becomes smeared shortly after the excitation. Using the diffusion coefficients obtained from the bimolecular recombination rates and 10 Å as an average separation distance between the radicals as an example value, we estimate that after 3 ps, the width of the distribution is ~10 Å (see note S7 in the supplementary material for details). To characterize the initial separation distance and its progression with time, sub-picosecond resolution at x-ray free electron lasers is required. The sensitivity of TRWAXS to the inter-radical separation distance is evident from the calculated signals for newly formed HgI/I radicals separated by distances of 10 and 15 Å, which correspond to the size of several acetonitrile molecules. The theoretical signals, along with the trace calculated for the infinite separation that corresponds to the dissociation signal at later time delays, are shown in Fig. 5. A comparison of these signals indicates that the proximity of radicals to each other results in emerging oscillations at q values below 2 $Å^{-1}$, which suggests that TRWAXS is indeed sensitive to the long scale inter-radical separation distance.

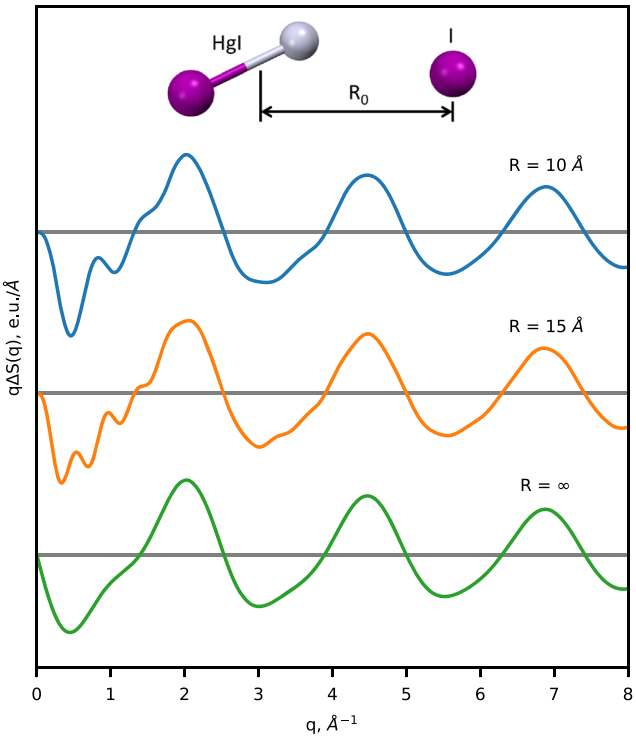

FIG. 5. Calculated solute-only TRWAXS signal as a function of distance R_0 between the I atom and the center of mass of the HgI radical. The simulation assumes R_0 being monodisperse and the HgI radical being randomly oriented with respect to the I atom.

CONCLUSIONS

In summary, we studied the recombination dynamics of radicals formed upon photodissociation of mercury halides HgX_2 (X = Br, I). Using complementary TRWAXS and OTA measurements, we observed a sub-nanosecond recombination process not reported before which we attribute to SGR, i.e., diffusion-limited geminate recombination. Specifically, we estimate that 68% of HgI/I and 50% of HgBr/Br pairs undergo rapid, biphasic decay on a time scale between 10 ps and 1 ns. Notably, the radicals produced in the three-body dissociation of $HgBr_2$, Hg and Br, do not exhibit the rapid concentration decay presumably due to their high mobility and potentially lower initial separation distance that made the fast process inaccessible within the temporal resolution of the reported experiments. In-depth understanding of the SGR process requires characterization of the time-dependent inter-radical distance distribution, which would be possible by TRWAXS with femtosecond time resolution at x-ray free electron lasers. This work suggests that mercury halides represent an important model system for studying SGR with femtosecond resolution because of the high amplitude of the scattering signals and the large reaction yield of SGR in acetonitrile. Future experiments will allow a quantitative comparison between kinetic and diffusion models for SGR, which will provide further insight into the validity of the macroscopic diffusion approach to solution reactivity on short time- and length-scales.

SUPPLEMENTARY MATERIAL

Supplementary material contains the details of TRWAXS data analysis, description of the equations used to fit the kinetic data, details of the thermodynamic analysis, and estimation of the time scale of inter-radical distance broadening for HgI_2.

ACKNOWLEDGMENTS

This work was supported by the Institute for Basic Science (IBS-R004). We thank Junbeom Jo and Sungjun Park for their assistance in the experiment.

REFERENCES

[1] B. J. Schwartz, J. C. King, J. Z. Zhang, and C. B. Harris, Chem. Phys. Lett. **203**, 503–508 (1993).
[2] K. J. Shin and R. Kapral, J. Chem. Phys. **69**, 3685 (1978).
[3] M. G. Hyde and G. S. Beddard, Chem. Phys. **151**, 239–248 (1991).
[4] T. W. Scott and S. N. Liu, J. Phys. Chem. **93**, 1393–1396 (1989).
[5] T. W. Scott and C. Doubleday, Jr., Chem. Phys. Lett. **178**, 9–18 (1991).
[6] A. L. Harris, J. K. Brown, and C. B. Harris, Annu. Rev. Phys. Chem. **39**, 341–366 (1988).

Published under license by AIP Publishing

[7]H. Ihee, M. Wulff, J. Kim, and S. Adachi, Int. Rev. Phys. Chem. **29**, 453–520 (2010).
[8]K. H. Kim, J. Kim, J. H. Lee, and H. Ihee, Struct. Dyn. **1**, 011301 (2014).
[9]A. B. Oelkers, L. F. Scatena, and D. R. Tyler, J. Phys. Chem. A **111**, 5353–5360 (2007).
[10]N. A. Borisevich, O. V. Buganov, V. L. Dubovskii, S. A. Tikhomirov, and G. B. Tolstorozhev, Opt. Spectrosc. **98**, 368–373 (2005).
[11]H. Kim, S. Shin, S. Lee, and K. J. Shin, J. Chem. Phys. **105**, 7705–7711 (1996).
[12]L. Milanesi, J. P. Waltho, C. A. Hunter, D. J. Shaw, G. S. Beddard, G. D. Reid, S. Dev, and M. Volk, Proc. Natl. Acad. Sci. U. S. A. **109**, 19563–19568 (2012).
[13]M. Volk, L. Milanesi, J. P. Waltho, C. A. Hunter, and G. S. Beddard, Phys. Chem. Chem. Phys. **17**, 762–782 (2015).
[14]A. B. Oelkers, E. J. Schutte, and D. R. Tyler, Photochem. Photobiol. Sci. **7**, 228–234 (2008).
[15]A. B. Stickrath, E. C. Carroll, X. Dai, D. A. Harris, A. Rury, B. Smith, K.-C. Tang, J. Wert, and R. J. Sension, J. Phys. Chem. A **113**, 8513–8522 (2009).
[16]J. Kim, K. H. Kim, K. Y. Oang, J. H. Lee, K. Hong, H. Cho, N. Huse, R. W. Schoenlein, T. K. Kim, and H. Ihee, Chem. Commun. **52**, 3734–3749 (2016).
[17]H. Hofmann and S. R. Leone, J. Chem. Phys. **69**, 3819–3825 (1978).
[18]T. K. Kim, M. Lorenc, J. H. Lee, M. Lo Russo, J. Kim, M. Cammarata, Q. Kong, S. Noel, A. Plech, M. Wulff, and H. Ihee, Proc. Natl. Acad. Sci. U. S. A. **103**, 9410–9415 (2006).
[19]S. Jun, J. H. Lee, J. Kim, J. Kim, K. H. Kim, Q. Kong, T. K. Kim, M. Lo Russo, M. Wulff, and H. Ihee, Phys. Chem. Chem. Phys. **12**, 11536 (2010).
[20]M. Volk, S. Gnanakaran, E. Gooding, Y. Kholodenko, N. Pugliano, and R. M. Hochstrasser, J. Phys. Chem. A **101**, 638–643 (1997).
[21]H. Bursing and P. Vohringer, Phys. Chem. Chem. Phys. **2**, 73–82 (2000).
[22]N. Pugliano, D. K. Palit, A. Z. Szarka, and R. M. Hochstrasser, J. Chem. Phys. **99**, 7273–7276 (1993).
[23]N. Pugliano, A. Z. Szarka, S. Gnanakaran, M. Triechel, and R. M. Hochstrasser, J. Chem. Phys. **103**, 6498–6511 (1995).
[24]J.-C. Labiche, O. Mathon, S. Pascarelli, M. A. Newton, G. G. Ferre, C. Curfs, G. Vaughan, A. Homs, and D. F. Carreiras, Rev. Sci. Instrum. **78**, 091301 (2007).
[25]K. Haldrup, M. Christensen, and M. M. Nielsen, Acta Crystallogr., Sect. A: Found. Crystallogr. **66**, 261–269 (2010).
[26]J. H. Lee, M. Wulff, S. Bratos, J. Petersen, L. Guerin, J.-C. C. Leicknam, M. Cammarata, Q. Kong, J. Kim, K. B. Møller, and H. Ihee, J. Am. Chem. Soc. **135**, 3255–3261 (2013).
[27]K. S. Kjær, T. B. van Driel, J. Kehres, K. Haldrup, D. Khakhulin, K. Bechgaard, M. Cammarata, M. Wulff, T. J. Sørensen, and M. M. Nielsen, Phys. Chem. Chem. Phys. **15**, 15003–15016 (2013).
[28]J. Lee, J. Kim, M. Cammarata, Q. Kong, K. H. Kim, J. Choi, T. Kim, M. Wulff, and H. Ihee, Angew. Chem., Int. Ed. **47**, 1047–1050 (2008).
[29]Q. Kong, J. H. Lee, M. Lo Russo, T. K. Kim, M. Lorenc, M. Cammarata, S. Bratos, T. Buslaps, V. Honkimaki, H. Ihee, and M. Wulff, Acta Crystallogr., Sect. A: Found. Crystallogr. **66**, 252–260 (2010).
[30]M. Lim, M. F. Wolford, P. Hamm, and R. M. Hochstrasser, Chem. Phys. Lett. **290**, 355–362 (1998).
[31]Y. Morino, Acta Crystallogr. **13**, 1107 (1960).
[32]Y. Morino, J. Nakamura, and P. W. Moore, J. Chem. Phys. **36**, 1050 (1962).
[33]G. Nagarajan, J. Mol. Spectrosc. **13**, 361–392 (1964).
[34]G. Winterhoff, S. C. Galleguillos Kempf, P. Jensen, and P. R. Bunker, J. Mol. Spectrosc. **354**, 71–82 (2018).
[35]P. F. de Violet, R. Bonneau, and J. Joussot-Dubien, Chem. Phys. Lett. **28**, 569–572 (1974).
[36]A. Treinin and E. Hayon, J. Am. Chem. Soc. **97**, 1716–1721 (1975).

Published under license by AIP Publishing